Electronic Supplementary Information

A Facile N-doped NiFe(B) (Oxy)Hydroxide Monolithic Electrode for Enhanced Water Oxidation

*Yushu Li [1, #], Huizhen Han [1, #], Xiuhang Wang [1], Yu Sun [1], Yulian Zhao [1], Shiyi Tao [1], Aoxing Duan [1], Yi Ma [1, *], Xin Bo [1, *], Zenglin Wang [1, *]*

1 Key Laboratory of Applied Surface and Colloid Chemistry, Ministry of Education, School of Chemistry and Chemical Engineering, Shaanxi Normal University, Xi' an 710119, China.

Author Contributions

# These authors contribute equally to this work.

Y. Li synthesised the materials and wrote the manuscript; H. Han responded the revision work with the help of Y. Zhao; X. Wang and Y. Sun helped the characterizations; A. Duan and S. Tao fabricated S-NiFe hydroxide materials; Y. Ma, X. Bo and Z. Wang supervised the project.

Experimental

Synthesis of NiCu porous substrate. Nickel meshs (NMs), nickel plates (NPs) and nickel foams (NFs) as the substrates were cut to the size of 0.5×2.0 cm^2, the substrates were cleaned by ultrasonication in 1.0 M HCl for 15 min and consequently washed with ultrapure water. This process was repeated 3 times and the pretreated substrates were stored in ethanol. A porous NiCu layer (denoted as NiCu/NM) was electrodeposited on NM to increase the surface roughness for the consequent electroless plating process in the electrolyte containing 1.0 mM $CuSO_4$, 5.0 mM $NiSO_4$, 5.0 mM H_3BO_3 and 3.0 M NH_4Cl. The electrodeposition lasts 60 s and the applied current density is 2.8 A cm^{-2}.

Synthesis of alloy NiFeB nuclei precursor. The NiFeB nuclei layer (denoted as NiFeB/NiCu/NM) was achieve on NiCu/NM through an electroless plating process. 1.26 mM $NiCl_2$ and 0.072 mM $FeSO_4$ were used as Ni and Fe sources, respectively. 0.26 mM $NaBH_4$ reductant was then added 5 ml ethanediamine (20%) and 0.019 mM $NaKC_4H_4O_6$ as complexing agents. The porous substrate was placed in the plating bath at 60℃ for 20 min with stirring.

Synthesis of N doped NiFe(B) (oxy)hydroxide monolithic electrode. The achieved NiFeB/NiCu/NM experienced a vaporization exchange process in an autoclave containing ammonia solution as NH_3 source under the temperature from 100 ℃ to 140 ℃ for 2~8 h to obtain the N doped NiFe(B) (oxy)hydroxide monolithic electrode (denoted as N-NiFeB/NiCu/NM). The synthetic scheme is also displayed in **Scheme 1**.

Synthesis of blank NiFe(B) (oxy)hydroxide monolithic electrode control sample. The NiFeB/NiCu/NM precursor experienced a vaporization exchange process in an autoclave containing KOH solution with the same pH as the ammonia solution under the temperature from 100 ℃ to 140 ℃ for 2~8 h. The control sample is denoted as NiFe(B).

Synthesis of S doped NiFe(B) based monolithic electrode. The achieved NiFeB alloy precursor on NF substrate was fabricated by the same protocol mentioned above (NiFeB/NF). Then the precursor electrode experienced a vaporization exchange process in an autoclave containing 0.6 g FeS in 2 mL H_2SO_4 (3 M) solution under 120 ℃ for 1 h obtain the S doped NiFe(B) based monolithic electrode (denoted as S-NiFeB/NF).

Physical characterization. The scanning electron microscopy (SEM, Hitachi SU8020) images and the elemental contributions were collected by X-ray energy dispersive spectrometry (EDX, Hitachi) with a 10 kV acceleration voltage. The X-ray diffraction (XRD) was measured by Philips X'Pert with Cu Kα radiation. The X-ray photoelectron spectroscopy (XPS) was carried out by Kratos AXIS ULTRA. Raman spectra were recorded on a Finder Vista spectrometer by using a 532 nm laser. To get rid of the effect of the nickel substrate, we applied

the coating process on carbon fibre paper (CFP) and the sample was dissolved in the nitrate acid for ICP-OES/MS (Agilent 5110, USA). By ICP-OES, the atomic ratio of Ni/Fe is 5.06, which is different from the initial addition in the electrolyte. This indicates that the rate of Fe deposition in this particular Ni/Fe electroless plating system is relatively slow, and this is also consistent with the previous reports.[1, 2]

Electrochemical characterization. The electrochemical measurements were measured with a CHI660D workstation **(**CHI) in a standard three-electrode system. The working electrode, the counter electrode and the reference electrode are the prepared electrode, a graphite rod and a saturated calomel electrode (SCE), respectively. The linear sweep voltammetries (LSVs) with a scan rate of 1 mV s^{-1} in 1.0 M KOH aqueous solution at room temperature were recorded until a stable cyclic voltammetries (CVs) presented and corrected with 95% *iR*-compensation. The test potential values (E_{SCE}) were converted to the reversible hydrogen electrode (E_{RHE}) using the following equation:

$$E_{RHE} = E_{SCE} + 0.2415 + 0.059\ \text{pH} \quad (1)$$

Tafel curves were also derived from LSVs based on the Tafel equation:

$$\eta = b \log j + a \quad (2)$$

Where j is the current density and b is the Tafel slope. The double layer capacitance (C_{dl}) was measured by cyclic voltammetry (CVs) in a non-Faradaic region with scanning rates of 10~200 mV s^{-1}. The electrochemical durability was obtained with chronopotentiometry (*p-t*) under the current density of 100 mA cm^{-2}. Electrochemical impedance spectroscopies (EISs) were performed in 1.0 M KOH solution in the frequency range of 0.01 Hz to 100 kHz, with AC voltage amplitude of 5 mV. The solution resistance (R_s), charge transfer resistance (R_{ct}) and the double layer capacitance values can be read and simulated by *Zsimp* software.

Figures

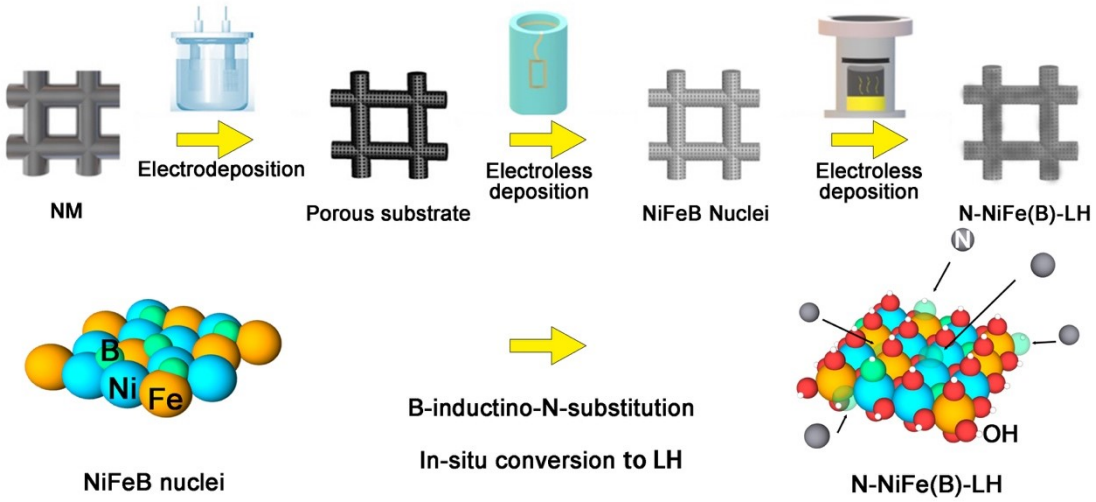

Scheme 1. Synthetic route to achieve N-NiFeB/NiCu/NM

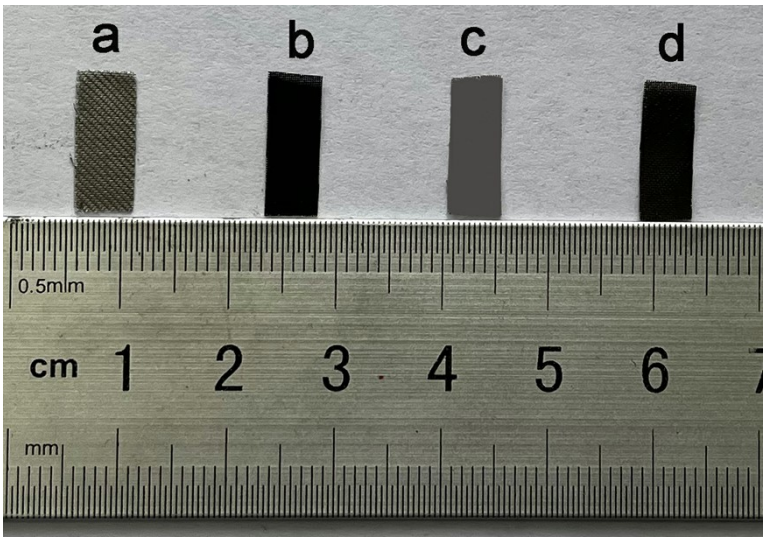

Fig.S1 Photos of (a) NM, (b) porous NiCu/NM substrate, (c) NiFeB/NiCu/NM and (d) N-NiFeB/NiCu/NM

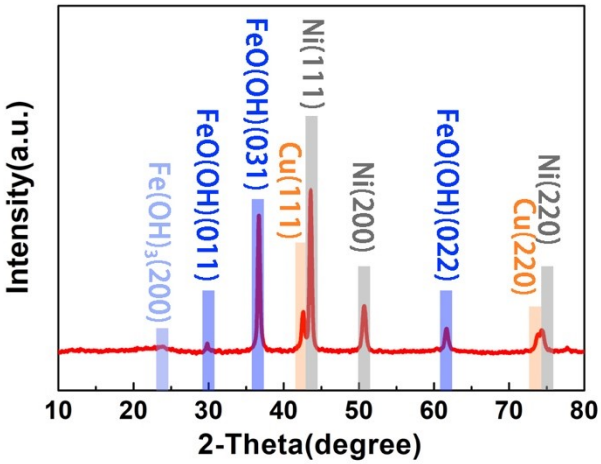

Fig.S2 XRD patterns of N-NiFeB/NiCu/NM.

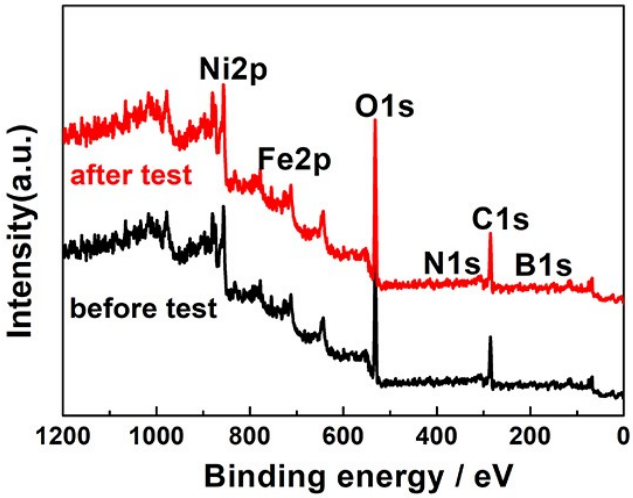

Fig.S3 Overall XPS survey of N-NiFeB/NiCu/NM.

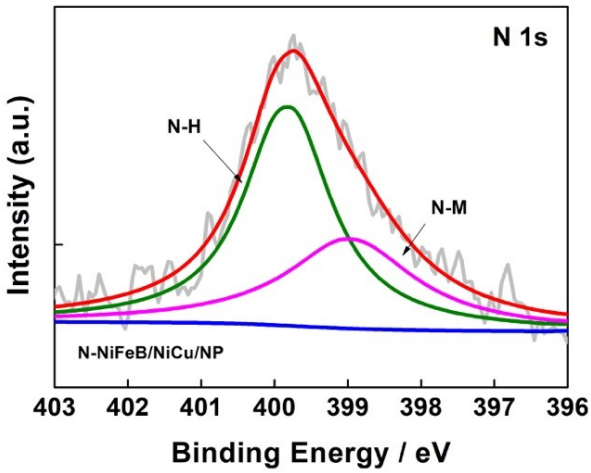

Fig.S4 HR-XPS data of N1s of N doped NiFe(B) (oxy)hydroxide on nickel plate substrate

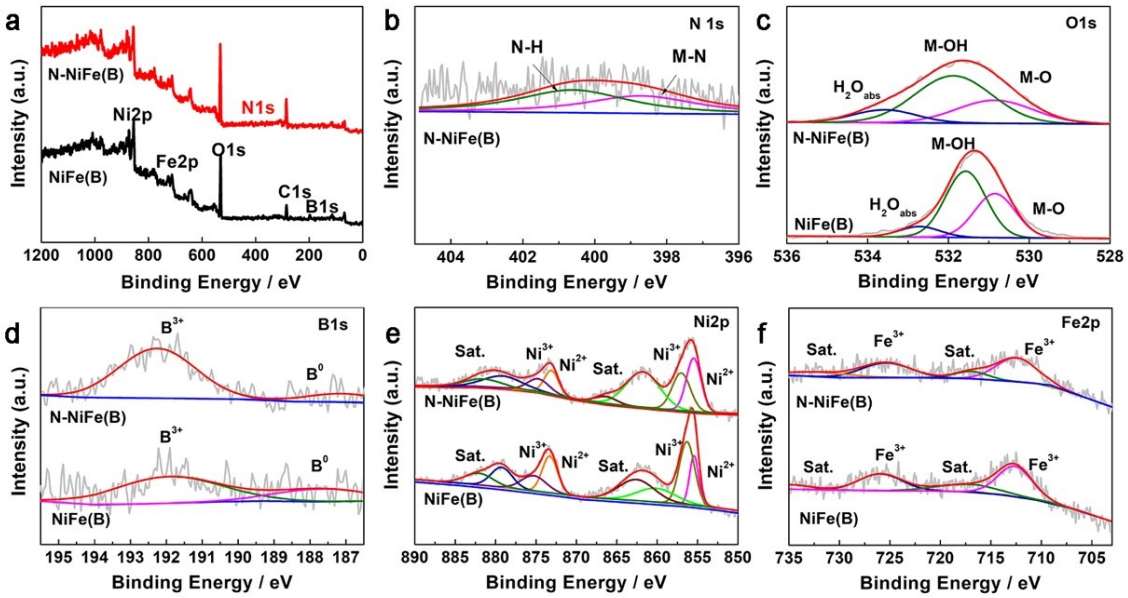

Fig.S5 XPS surveys (a) of N1s (b), O1s (c), B1s (d), Ni2p (e) and Fe2p (f) in the N-NiFe(B)/NiCu/NM and NiFe(B)/NiCu/NM (Steamed in alkaline without NH_3).

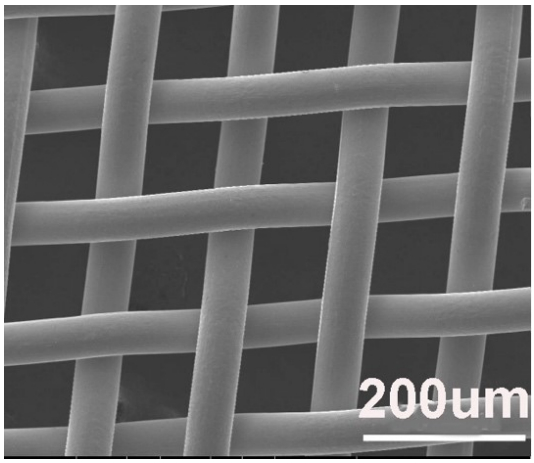

Fig.S6 SEM photo of bared NM substrate.

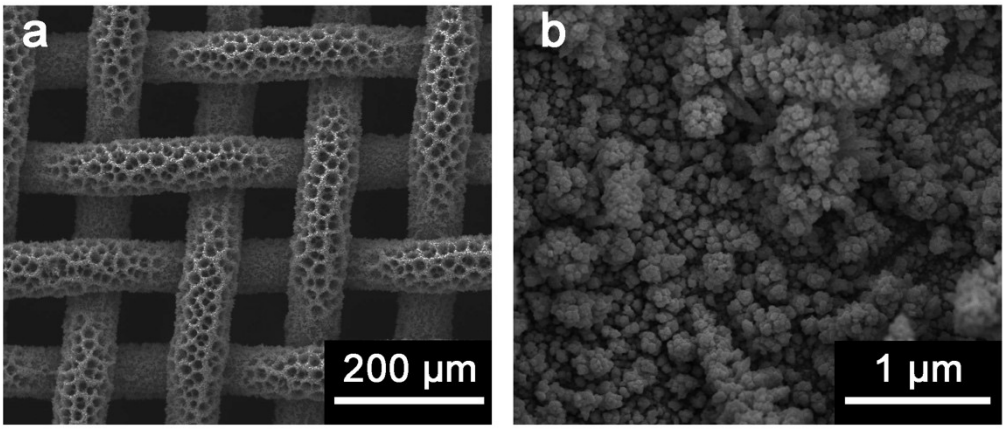

Fig.S7 SEM photo of porous NiCu/NM.

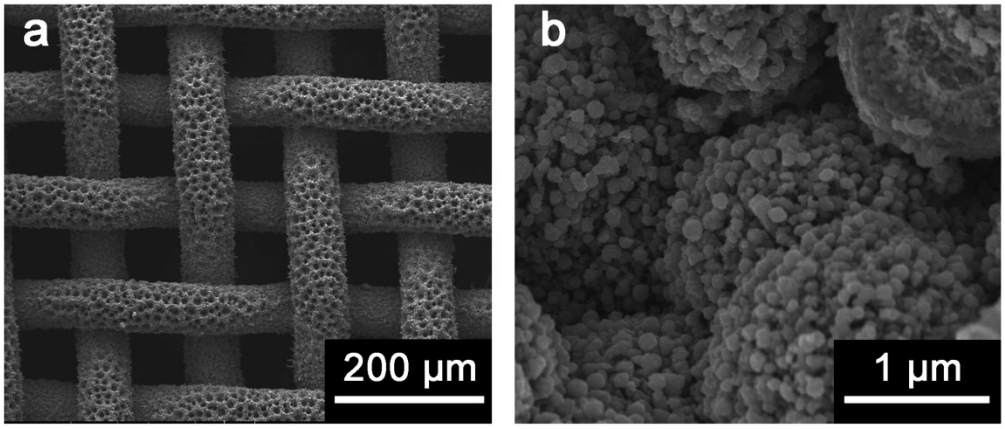

Fig.S8 SEM photo of NiFeB/NiCu/NM.

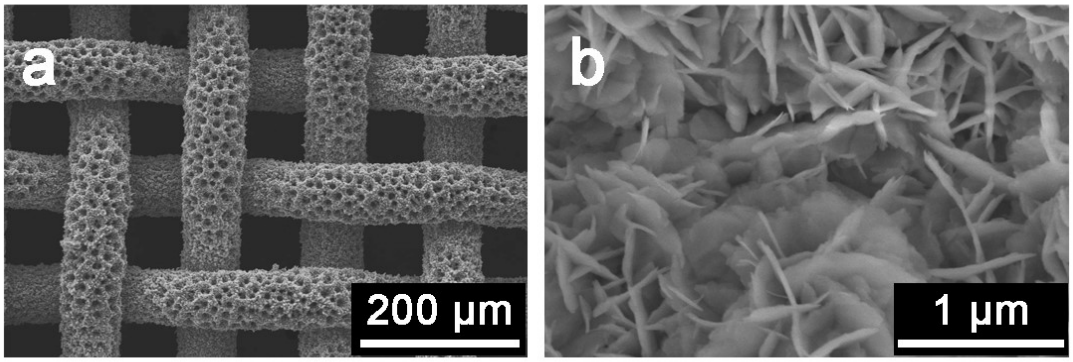

Fig.S9 SEM photo of N-NiFeB/NiCu/NM.

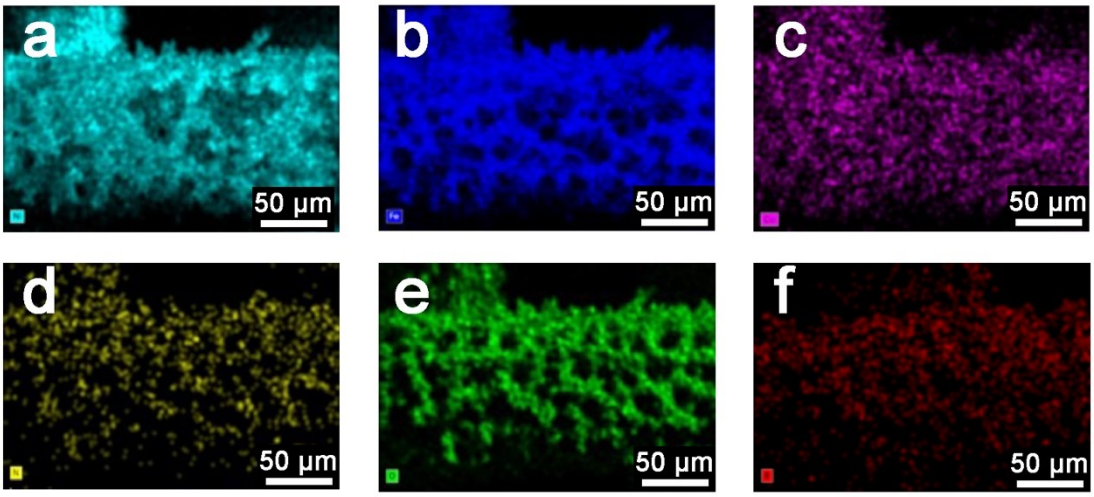

Fig.S10 EDS mappings of Ni (a), Fe (b), Cu (c), N (d), O (e), B (f) on N-NiFeB/NiCu/NM.

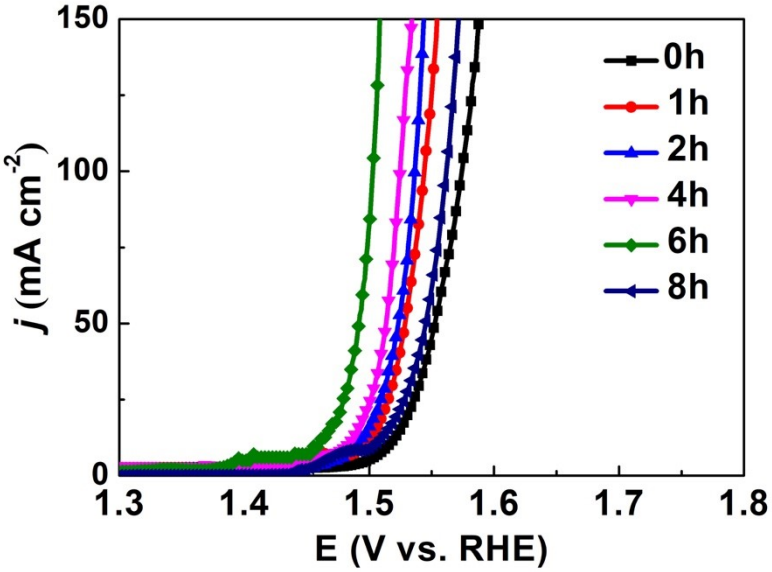

Fig.S11 The LSVs of N-NiFe/NiCu/NM electrodes prepared by various NH_3 vaporization time.

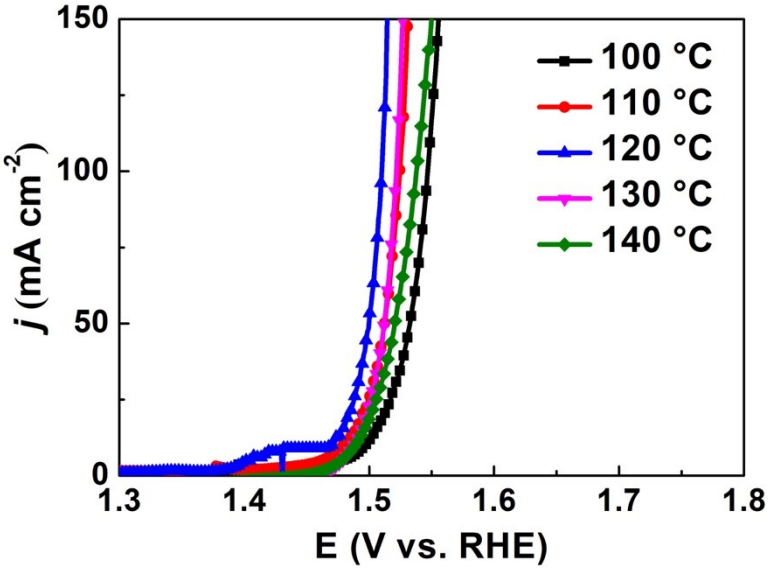

Fig.S12 The LSVs of N-NiFe/NiCu/NM electrodes prepared at various NH_3 vaporization temperatures.

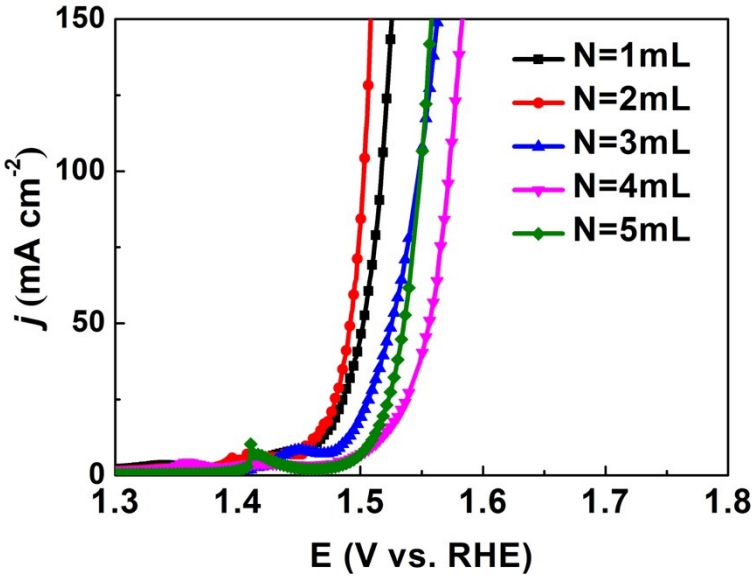

Fig.S13 The LSVs of N-NiFe/NiCu/NM electrodes prepared at various ammonia solution addition.

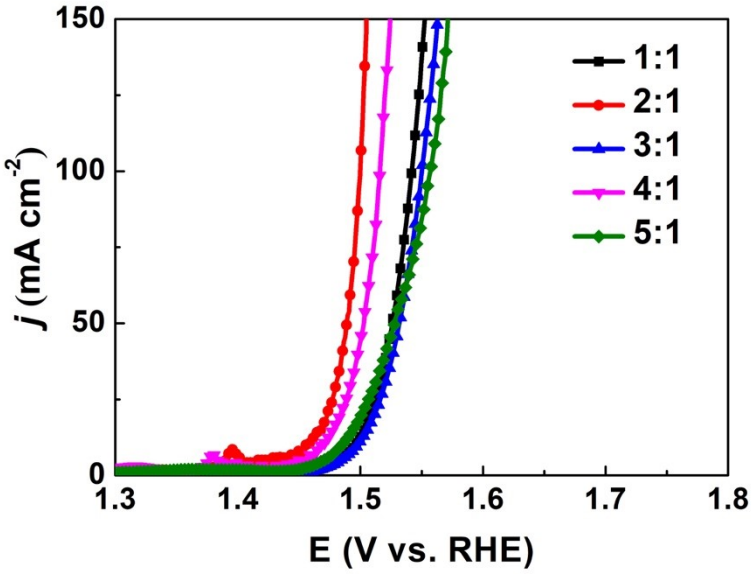

Fig.S14 The LSVs of N-NiFe/NiCu/NM electrodes prepared at various Ni/Fe ratios in NiFeB nuclei.

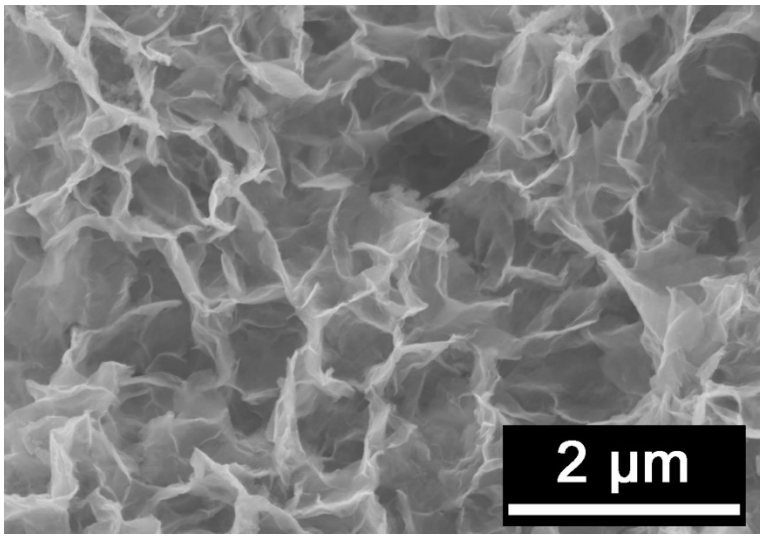

Fig.S15 SEM photo of N-NiFeB/NiCu/NM after durability test.

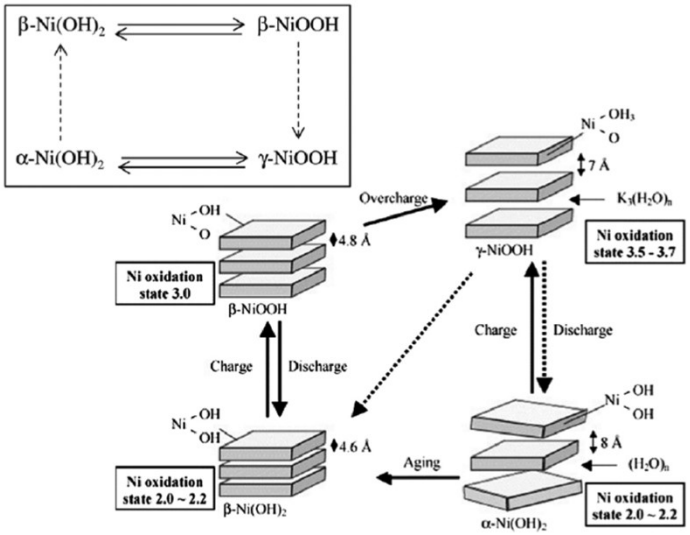

Fig.S16 Reused figure from the literature[3]. The change of Ni oxidation states and structures under the applied oxidation potential.

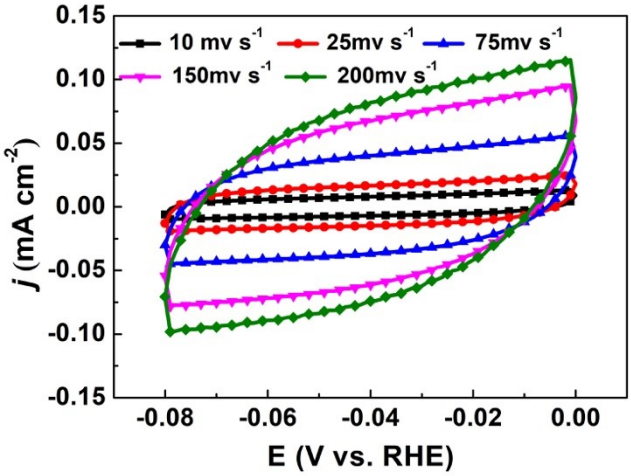

Fig.S17 CVs of bared NM substrate at various scanning ramps during non-Faradaic zone to measure the electrochemical active surface area.

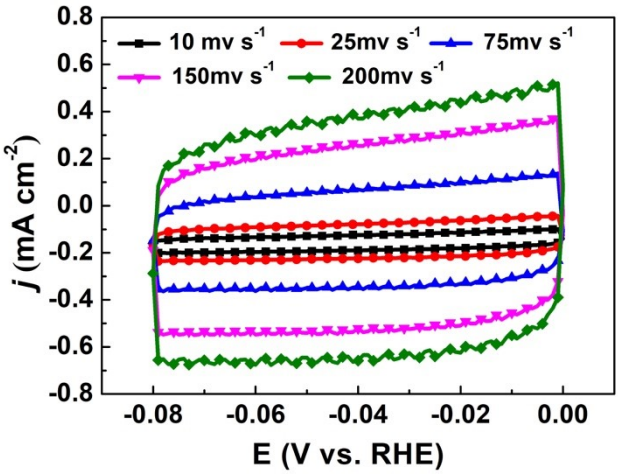

Fig.S18 CVs of porous NiCu/NM substrate at various scanning ramps during non-Faradaic zone to measure the electrochemical active surface area.

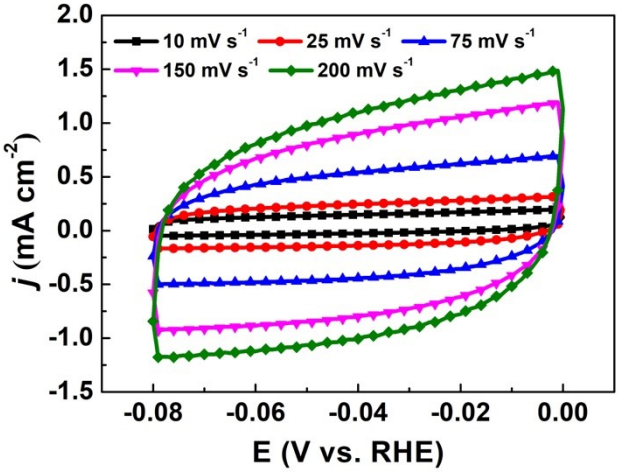

Fig.S19 CVs of NiFeB/NiCu/NM at various scanning ramps during non-Faradaic zone to measure the electrochemical active surface area.

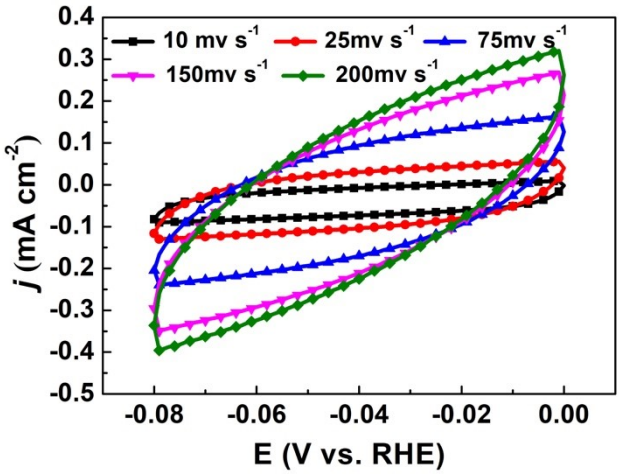

Fig.S20 CVs of N-NiFeB/NM without porous NiCu framework at various scanning ramps during non-Faradaic zone to measure the electrochemical active surface area.

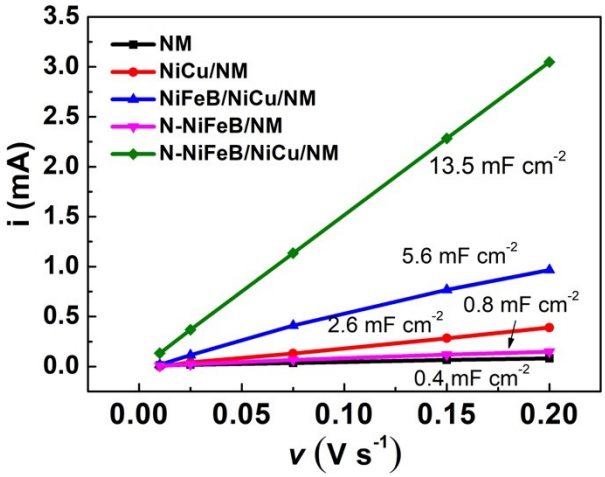

Fig.S21 C_{dl} values derived from **Fig.2f** and **Fig.S16~S19**.

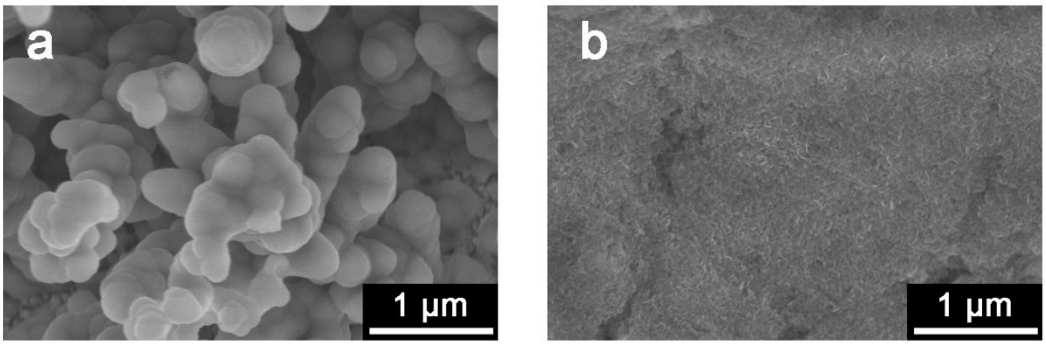

Fig.S22 SEM images of (a) NiFe/NiCu/NM and (b) N-NiFe/NiCu/NM without B inductor in galvanic-plating nuclei layer.

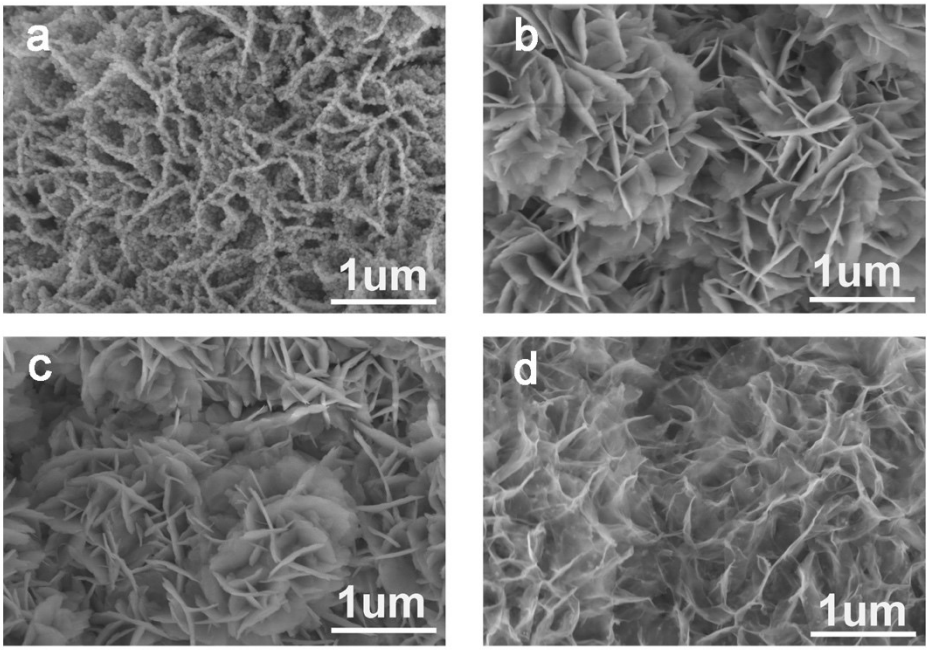

Fig.S23 The SEM images of N-NiFeB/NiCu//NM with different NH_3 modified time: (a) 2 hours, (b) 4 hours, (c) 6 hours, (d) 8 hours.

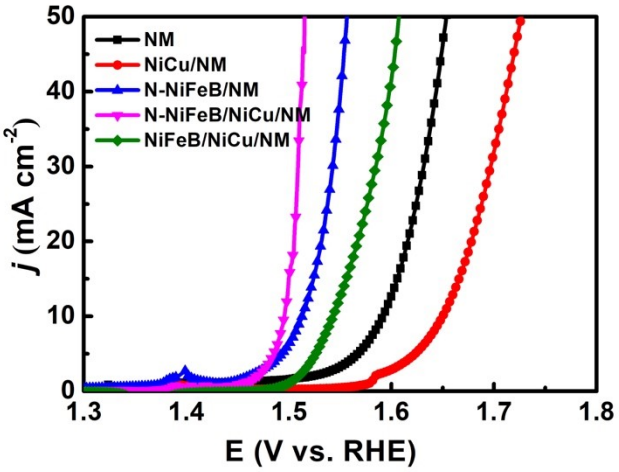

Fig.S24 ECSA normalized OER polarization curves of N-NiFeB/NiCu/NM and the control samples.

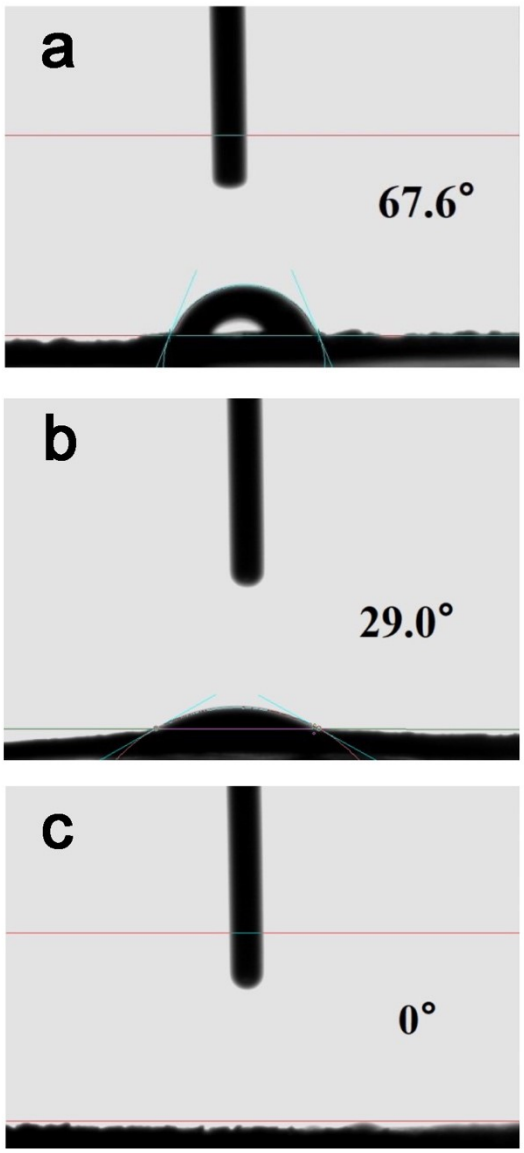

Fig.S25 Surface contact angle measurement of (a) NP, (b) NiFeB/NP and (c) N-NiFeB/NP.

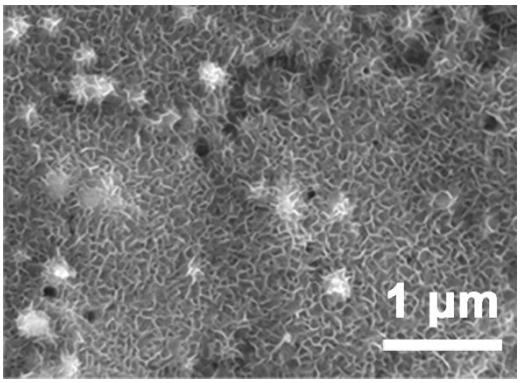

Fig.S26 The SEM image of S-NiFeB/NF

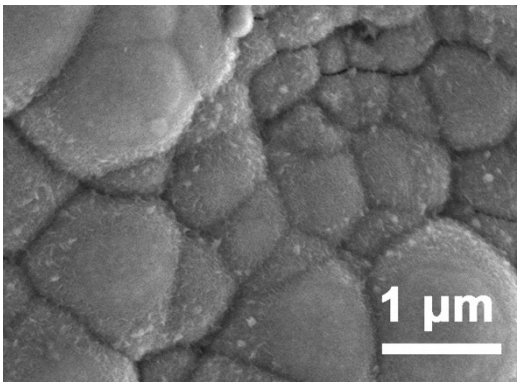

Fig.S27 The SEM image of NiFeB/NF

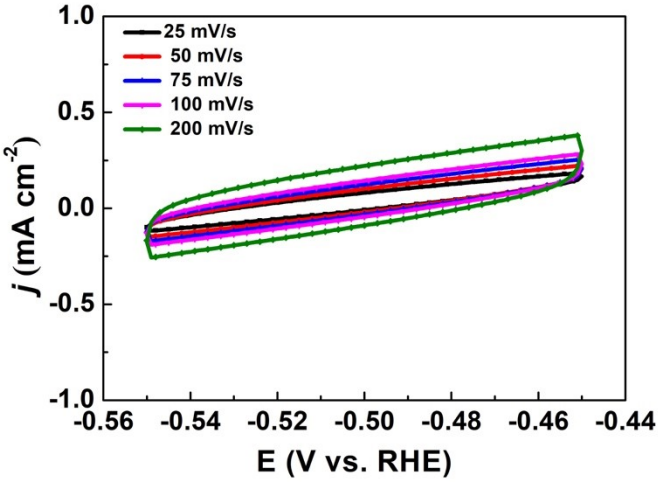

Fig.S28 CVs of NiFeB/NF at various scanning ramps during non-Faradaic zone to measure the electrochemical active surface area.

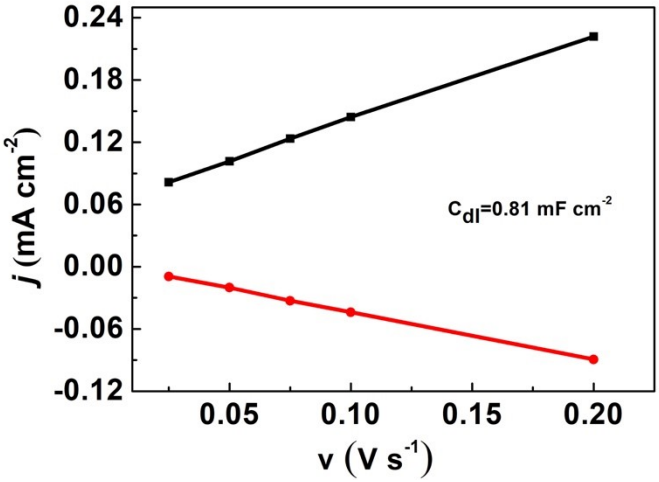

Fig.S29 C_{dl} values derived from **Fig.S27**.

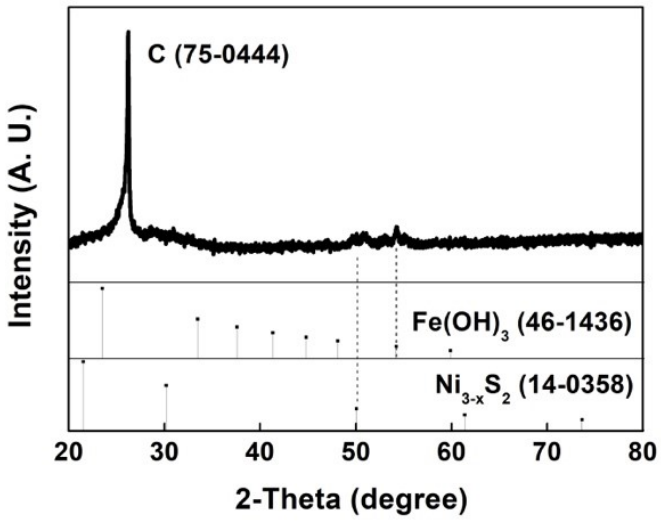

Fig.S30 XRD patterns of S-NiFeB/NF.

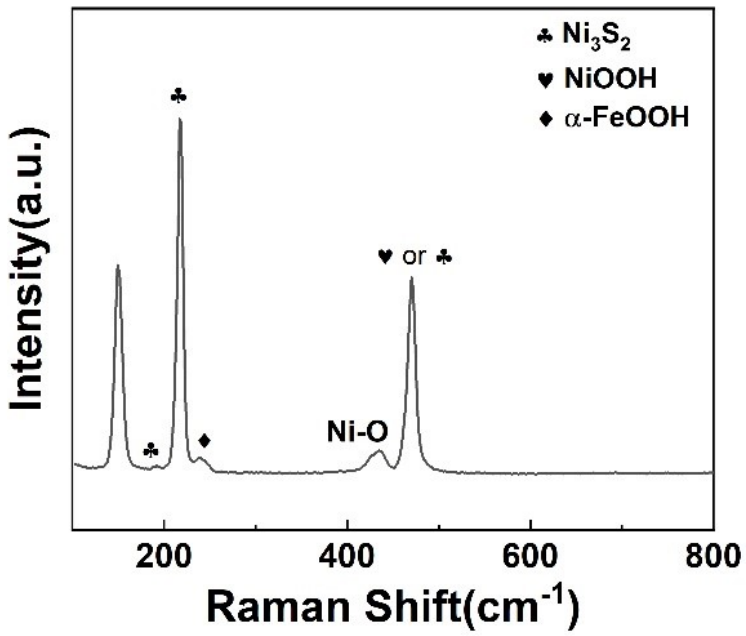

Fig.S31 Raman shift of S-NiFeB/NF.

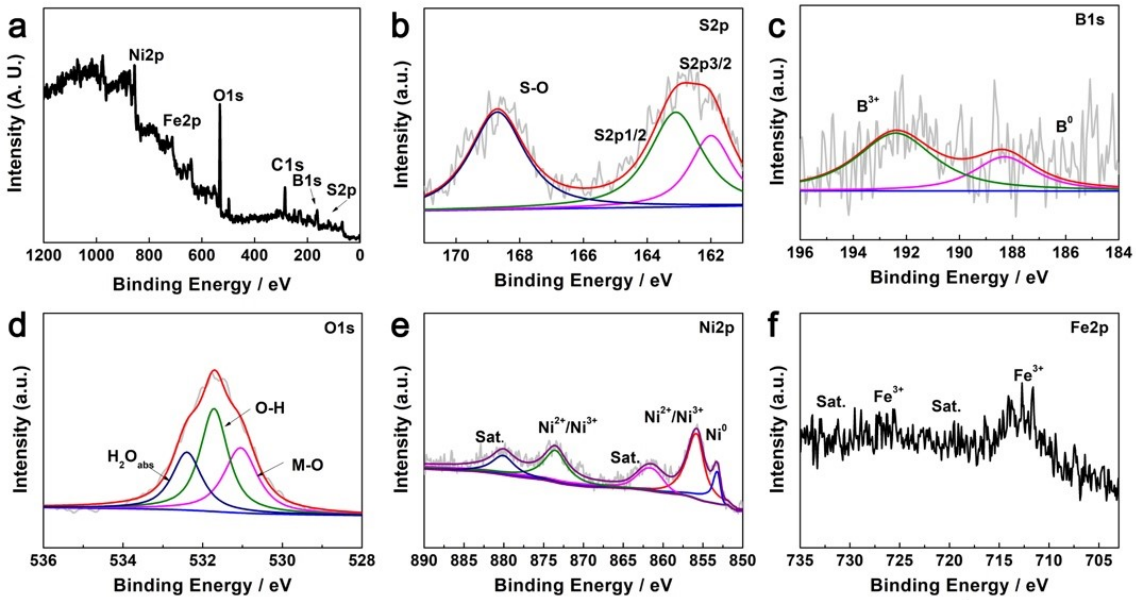

Fig.S32 XPS data of S-NiFe(B)/NF: (a) overall survey; (b) S2p; (c) B1s; (d) O1s; (e) Ni2p; (f) Fe2p.

As S modifies the surface, the micro-morphology roughened obviously (**Fig.S26~S27**), displaying a coral-like structure (**Fig.S26**) of S-NiFeB/NF, leading to the increase of the ECSA consequently (**Fig.3d~3e** and **Fig.S28~S29**). The XRD patterns (**Fig.S30**) prove the existance of $Fe(OH)_3$ and $Ni_{3-x}S_2$. The Raman shifts (**Fig.S31**) at 189 and 217 cm^{-1} are assigned to Ni-S bonds, corresponding to the vibrational peaks of Ni_3S_2.[4] The characteristic peak at 242 cm^{-1} can be ascribed to the Fe-O bond of α-FeOOH.[5] The signal at 435 cm^{-1} can be attributed to Ni-O.[6] There is a peak at 470 cm^{-1} can be identified as either Ni_3S_2 or Ni-OH of $Ni(OH)_2$.[7] Then, XPS data display more information on electronic structure. The XPS spectra of S-NiFeB/NF confirms the Ni, Fe, B, S, and O contents (**Fig.S32**). The S2p region (**Fig.S32b**) shows three peaks at 161.9, 163 and 168.9 eV corresponding to the S-Ni signals in Ni_3S_2 and S-O, respectively.[8-10] Similarly, the XPS spectra of the B1s region for S-NiFeB/NF shows two characteristic peaks located at 191.4 eV and 188.3 eV which can be assigned to the oxidised borate species and zero-valent boron (**Fig.S32c**).[11] In **Fig.S32d**, the O1s peak of S-NiFe(B)/NF sample also presents a typical (oxy)hydroxide structure and metal oxide species. In the Ni2p spectra (**Fig.S32e**), the peaks are divided into two spin-orbit doublets, which are indexed to $Ni2p_{3/2}$ and $Ni2p_{1/2}$ of Ni^{2+} and Ni^{3+} states, respectively.[12] The two satellite sub-peaks are located at 861.9 eV and 880.1 eV. the peak at 854.1 eV corresponds to metallic Ni.[13] The Fe 2p shows two main peaks, 710.5 eV for Fe $2p_{3/2}$ and 723.0 eV for $Fe2p_{1/2}$, matching well with the characteristics of Fe^{3+} in S-NiFe(B)/NF (**Fig.S32f**).[14]

Tables

Table S1 Electrocatalytic performance of N-NiFeB/NiCu/NM and other reported electrocatalysts in basic electrolytes for water splitting recently.

Catalysts	J (mA $cm^{-2)}$	η (mV)	Tafel slop (mV dec^{-1})	Refs.
N-NiFeB/NiCu/NM	10	223	39	This work
NiFeB@NiFeBi	10	237	58	[15]
NiFeLDH@CNT	10	290	31	[16]
$NiFeS_2$	10	286	56.3	[17]
CoB@CoBi	10	291	50.73	[18]
NiFe/N-TiO_2	10	235	48.9	[19]
Hcp-NiFe@NC	10	226	41	[20]
N2-NiFe-PBA/NCF	50	270	70	[21]
NiFe-LH/Co,N-CNF	10	312	60	[22]
NiFeB/rGO	15	230	50	[23]
Cox-FeB	10	298	62.6	[24]
NixB/NF	20	280	-	[25]
$NiB_{0.45}$/Cu	10	296	58	[26]

Table S2. Summary of EIS fitted parameters for NM, NiCu/NM, NiFeB/NiCu/NM, N-NiFeB/NM, N-NiFeB/NiCu/NM, RuO_2/NM for OER in 1 M KOH.

Electrodes	R_s (ohm)	R_{ct} (ohm)	C_{dl} (mF cm^{-2})
NM	1.62	77.92	0.67
N-NiFeB/NiCu/NM	1.66	1.36	43
NiFeB/NiCu/NM	1.49	2.22	9.6
NiCu/NM	1.51	9.00	1.52
RuO_2/NM	1.85	4.19	0.73

References

1. V. Torabinejad, M. Aliofkhazraei, S. Assareh, M. H. Allahyarzadeh and A. S. Rouhaghdam, *J. Alloys Compd.*, 2017, **691**, 841-859.
2. J. Zhang, Z. Liu, S. Ma, Y. Zhou and J. Xia, presented in part at the 2011 International Conference on Remote Sensing, Environment and Transportation Engineering, Nanjing, 2011.
3. F. Dionigi and P. Strasser, *Adv. Energy Mater.*, 2016, **6**, 1600621.
4. M. Kajbafvala, K. Rahimi, B. Eshqi, O. Moradlou, N. Sarikhani and A. Z. Moshfegh, *ACS Appl. Nano Mater.*, 2023, **6**, 21556-21570.
5. M. Chen, Y. Zhang, J. Chen, R. Wang, B. Zhang, B. Song and P. Xu, *Small*, 2024, e2309371.
6. J. Wu, M. Hou, Z. Chen, W. Hao, X. Pan, H. Yang, W. Cen, Y. Liu, H. Huang, P. W. Menezes and Z. Kang, *Adv. Mater.*, 2022, **34**, e2202995.
7. D. Li, W. Wan, Z. Wang, H. Wu, S. Wu, T. Jiang, G. Cai, C. Jiang and F. Ren, *Adv. Energy Mater.*, 2022, **12**.
8. X. Luo, P. Ji, P. Wang, X. Tan, L. Chen and S. Mu, *Adv. Sci.*, 2022, **9**, e2104846.
9. D. Li, W. Wan, Z. Wang, H. Wu, S. Wu, T. Jiang, G. Cai, C. Jiang and F. Ren, *Adv. Energy Mater.*, 2022, **12**, 2201913.
10. X. Chen, Y. Cheng, Y. Wen, Y. Wang, X. Yan, J. Wei, S. He and J. Zhou, *Adv. Sci.*, 2022, **9**, e2204742.
11. W. Hong, S. Sun, Y. Kong, Y. Hu and G. Chen, *J. Mater. Chem. A*, 2020, **8**, 7360-7367.
12. J. Zhao, N. Liao and J. Luo, *J. Mater. Chem. A*, 2023, **11**, 9682-9690.
13. C. Chang, S. Zhu, X. Liu, Y. Chen, Y. Sun, Y. Tang, P. Wan and J. Pan, *Ind. Eng. Chem. Res.*, 2021, **60**, 2070-2078.
14. P. Thangavel, M. Ha, S. Kumaraguru, A. Meena, A. N. Singh, A. M. Harzandi and K. S. Kim, *Energy Environ. Sci.*, 2020, **13**, 3447-3458.
15. P. Han, T. Tan, F. Wu, P. Cai, G. Cheng and W. Luo, *Chinese Chem. Lett.*, 2020, **31**, 2469-2472.
16. M. Gong, Y. Li, H. Wang, Y. Liang, J. Z. Wu, J. Zhou, J. Wang, T. Regier, F. Wei and H. Dai, *J. Am. Chem. Soc.*, 2013, **135**, 8452-8455.
17. B. Q. Li, S. Y. Zhang, C. Tang, X. Cui and Q. Zhang, *Small*, 2017, **13**, 1700610.
18. T. Tan, P. Han, H. Cong, G. Cheng and W. Luo, *ACS Sustain. Chem. Eng.*, 2019, **7**, 5620-5625.
19. X. Liu, Z. Chen and M. Cao, *ACS Appl. Energy Mater.*, 2019, **2**, 5960-5967.

20. C. Wang, H. Yang, Y. Zhang and Q. Wang, *Angew. Chem. Int. Ed. Engl.*, 2019, **58**, 6099-6103.
21. C. Lai, H. Li, Y. Sheng, M. Zhou, W. Wang, M. Gong, K. Wang and K. Jiang, *Adv. Sci.*, 2022, **9**, e2105925.
22. Q. Wang, L. Shang, R. Shi, X. Zhang, Y. Zhao, G. I. N. Waterhouse, L. Z. Wu, C. H. Tung and T. Zhang, *Adv. Energy Mater.*, 2017, **7**, 1700467.
23. J. M. V. Nsanzimana, R. Dangol, V. Reddu, S. Duo, Y. Peng, K. N. Dinh, Z. Huang, Q. Yan and X. Wang, *ACS Appl. Mater. Interfaces*, 2019, **11**, 846-855.
24. H. Chen, S. Ouyang, M. Zhao, Y. Li and J. Ye, *ACS Appl. Mater. Interfaces*, 2017, **9**, 40333-40343.
25. J. Masa, I. Sinev, H. Mistry, E. Ventosa, M. de la Mata, J. Arbiol, M. Muhler, B. Roldan Cuenya and W. Schuhmann, *Adv. Energy Mater.*, 2017, **7**, 1700381.
26. J. Jiang, M. Wang, W. Yan, X. Liu, J. Liu, J. Yang and L. Sun, *Nano Energy*, 2017, **38**, 175-184.